# Assessment of non-rigid body, direction- and velocity-dependent error motions and their cross-talk by two-dimensional digital scale measurements at multiple positions

Soichi Ibaraki[a], Mashu Hiruya[b]

[a]*Department of Mechanical Systems Engineering, Hiroshima University*
*Kagamiyama 1-4-1, Higashi Hiroshima, 739-8527, Japan. Phone/Fax: +81-82-424-7580*
[b]*Department of Micro Engineering, Kyoto University*
*Katsura, Nishigyo-ku, Kyoto 616-8540, Japan*

*Type of contribution: Original research paper*

**Abstract**

The conventional volumetric error compensation for a machine tool is based on the machine's kinematic model, which formulates the tool center point (TCP) position based on the assumption of rigid-body motion of each axis. Particularly in large-sized machine tools, error motions that do not satisfy this assumption may have a significant impact on the machine's overall volumetric accuracy. In addition to position-dependent quasi-static error motions included in the conventional kinematic model, this paper proposes a scheme to assess quasi-static cross-talk between axes and direction- and velocity-dependent error motions. This paper proposes test procedures to measure two dimensional (2D) contour error trajectories by using a 2D digital scale (cross grid encoder). Unlike many previous works, this paper proposes to perform the tests at multiple positions over the machine tool's entire workspace, and the error motions are assessed by comparing contour error profiles. An experimental case study on a large-sized bridge-type vertical machine tool

*Email address:* ibaraki@hiroshima-u.ac.jp (Soichi Ibaraki)

shows that such influences can be significant error contributors. The proposed tests can assess error motions only at discrete points where a 2D digital scale is installed. It can be applied as accuracy inspection to "roughly" assess the machine's volumetric accuracy by using a 2D digital scale only, but it is generally not for the compensation.

*Keywords:* machine tool, two-dimensional digital scale, cross grid encoder, volumetric accuracy, measurement, kinematic model

---

## 1. Introduction

Many latest commercial CNC (computerized numerical control) systems can numerically compensate for volumetric errors, e.g. Siemens [1] and Fanuc [2]. In ISO 230-1 [3], revised in 2012, defines the term "volumetric accuracy" that represents the range of the three-dimensional (3D) positioning error of a machine tool over the entire workspace. ISO/TR 16907 [4] was published in 2015 describing numerical compensations for machine tool volumetric errors.

Typical machine tools have three (X, Y and Z) or more linear axes. Each linear axis has six error motions (linear positioning, straightness, and angular error motions) [3]. When the tool center point (TCP) is positioned at an arbitrary point in the workspace, all of these error motions are superimposed onto the TCP's 3D position error. In many commercial volumetric error compensations, the machine's kinematic model is adopted to calculate this superposition of error motions and then to modify the command position to cancel its influence. The kinematic modelling of a machine tool has been studied since the 1980s [5]. Since then, many papers, including recent ones [6, 7, 8], have presented the volumetric error compensation based on the kinematic model. The kinematic model plays a core role not only in the compensation, but also in "indirect" measurement of error motions. When the position error at the TCP is somehow measured by using e.g. a ball bar [9], a tracking interferometer [10], a touch-triggered probe [11], a two-dimensional (2D) digital scale [12], or a machining test [13], then error motions of all the axes can be numerically identified by inversely solving the kinematic model. A review can be found in [14, 15].

The kinematic model assumes the rigid-body motion of each axis; its formulation will be presented in Section 2.1. Particularly in large-sized machine tools [16], error motions that do not satisfy this rigid-body assumption may have a significant impact on the machine's overall volumetric accuracy. ISO/TR 16907 [4] presents such an example shown in Fig. 1. The angular error motion of Y-axis (spindle-head slide), $E_{AY}$, may vary as a function of

the position of the Z-axis (ram), due to the finite stiffness of the column, its connection to the bed, the bed itself, and its connection to the foundation [4]. This example shows a case where the position of one linear axis influences error motions of the other axis carrying it. Such a "cross-talk" influence cannot be described by the conventional kinematic model. Some past works [17, 18] discussed such a "cross-talk" but they mostly focused on the dynamic vibration. A main focus of this paper is on the assessment of quasi-static error motions induced by this cross-talk.

Furthermore, direction- and velocity-dependent error motions often have significant influence on the overall volumetric accuracy particularly on large-sized machines, but they are typically not included on the conventional kinematic model. Almost all commercial CNC systems can compensate for direction-dependent linear positioning deviations, often called the "backlash." On large machines, angular error motions can be direction-dependent. The inclusion of such an influence into the kinematic model, as well as its assessment scheme, is also this paper's original contribution.

To assess 1) quasi-static cross-talk between the axes, 2) direction- and 3) velocity-dependent error motions, this paper proposes test procedures to measure a set of 2D contouring error profiles at multiple positions over the entire workspace. ISO 230-1 [3], and the corresponding machine-specific standards, e.g. ISO 10791-1 [19] for horizontal machining centers, describe test procedures to assess all quasi-static error motions of linear axes. They do not include the tests to observe error motions under axis "cross-talk."

This paper employs a 2D digital scale (the term in [3]), or a cross grid encoder [12]. Past works [12, 20, 21] used a 2D digital scale but their schemes can be seen essentially the same as the tests in ISO 230-1 [3]. When a 2D digital scale is used, the measuring range is limited to the size of the reference grid, which is typically 200 to 300 mm in diameter (see Table 3). This paper proposes measuring 2D error profiles at multiple locations over the entire workspace. It enables to assess angular error motions over the distance between the two tests. This assessment is one of this paper's original

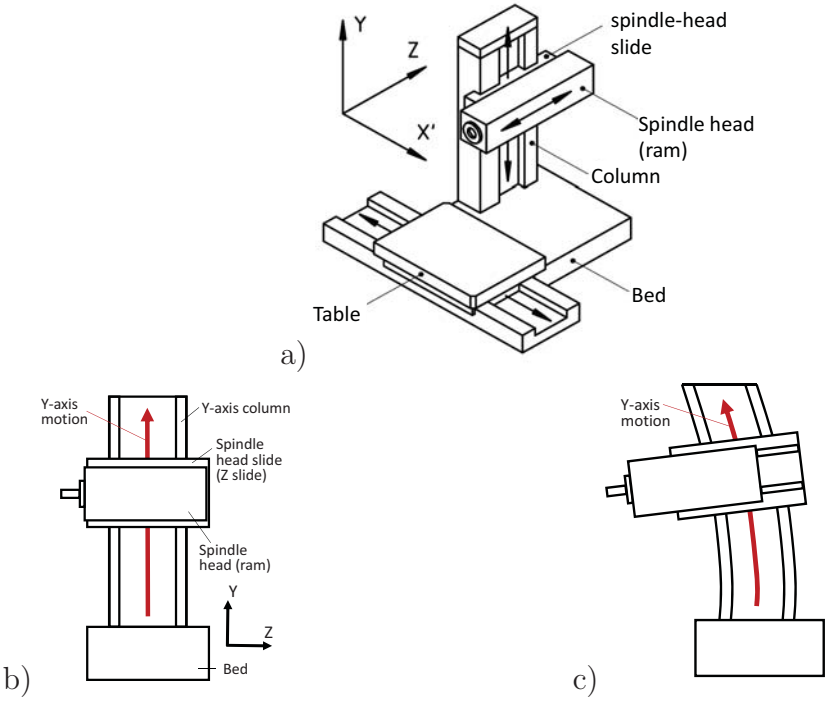


Figure 1: An example of possible non-rigid body behavior of a Y-axis carrying a heavy Z-axis ram [4], a) example machine configuration [4], b) when the ram's center of gravity is near the column, and c) when the ram goes out to -Z direction.

contributions.

## 2. Error motions to be assessed

This paper considers a bridge-type vertical machine configuration shown in Fig. 2. Basic idea of this paper can be extended to any machine configurations. After reviewing the conventional rigid-body kinematic model in Section 2.1, the following subsections will present the error motions that this paper proposes to assess.

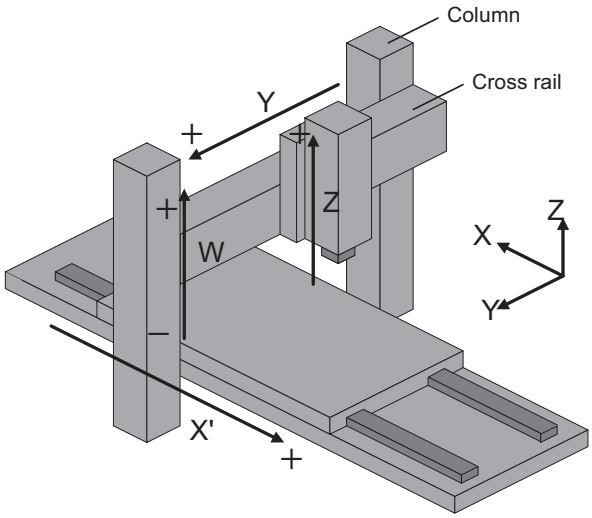


Figure 2: Machine configuration targeted in this paper.

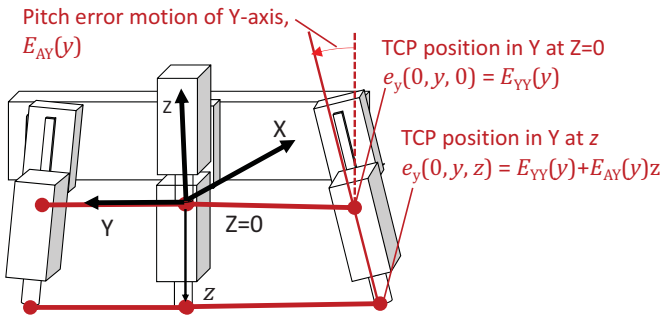


Figure 3: Influence of pitch error motion of Y-axis, $E_{AY}(y)$, on the positioning error in the Y-direction, when the Z-axis is positioned at $z$. Such a rigid-body influence is included in the conventional kinematic model (1).

### *2.1. Quasi-static position-dependent error motions: Error motions contained in conventional rigid-body kinematic model*

The derivation of the conventional kinematic model has been presented in many previous publications (see Section 1) and thus it is reviewed here only briefly. For the machine in Fig. 2, the conventional kinematic model is

given by:

$$\begin{aligned} e_x(x,y,z) &= E_{XX}(x) + E_{XY}(y) + E_{XZ}(z) \\ &\quad - \left(E_{CX}(x) + E_{C(0X)Y}\right) y - \left(E_{BX}(x) + E_{BY}(y) + E_{B(0X)Z}\right) z \\ e_y(x,y,z) &= E_{YX}(x) + E_{YY}(y) + E_{YZ}(z) \\ &\quad + E_{CX}(x) \cdot x - \left(E_{AX}(x) + E_{AY}(y) + E_{A(0Y)Z}\right) z \\ e_z(x,y,z) &= E_{ZX}(x) + E_{ZY}(y) + E_{ZZ}(z) - E_{BX}(x) \cdot x + E_{AX}(x) \cdot y \end{aligned} \quad (1)$$

where $(e_x(x,y,z), e_y(x,y,z), e_z(x,y,z))$ represents the 3D position error at the TCP for the command position $(x,y,z)$. Each axis, for example X-axis, has the linear positioning error motion, $E_{XX}(x)$, straightness error motions in Y and Z, $E_{YX}(x)$ and $E_{ZX}(x)$, and angular error motions around X, Y, and Z-axes, $E_{AX}(x)$, $E_{BX}(x)$ and $E_{CX}(x)$. See ISO 230-1 [3] for these notations.

It is emphasized that the conventional kinematic model (1) only contains quasi-static error motions that are dependent on the axis' linear position. The notation, e.g. $E_{XX}(x)$, represents a function of the command linear position, $x$.

Figure 3 illustrates the kinematic influence included in this model. As an example, the pitch error motion of Y-axis, $E_{AY}(y)$, changes the direction of Z-axis, mounted on the Y-axis, and consequently causes the positioning error in the Y-direction, $e_y$, when the Z-axis is positioned at $z$ (this influence is included in the second equation in Eq. (1)). Here, both Y- and Z-axes are assumed a rigid-body. $E_{AY}(y)$ changes the direction of the Z-axis average line only. All the error motions of Z-axis are identical at any Y position. Similarly, all the error motions of Y-axis are identical at any Z positions.

*2.2. Quasi-static cross-talk between axes*

In the conventional kinematic model (1), when the Z-axis is mounted on the Y-axis, the Z-axis position does not influence the Y-axis error motions. The example in Fig. 1 shows the case where the Z-axis position can affect the Y-axis error motions, due to the elastic deformation of e.g. the column.

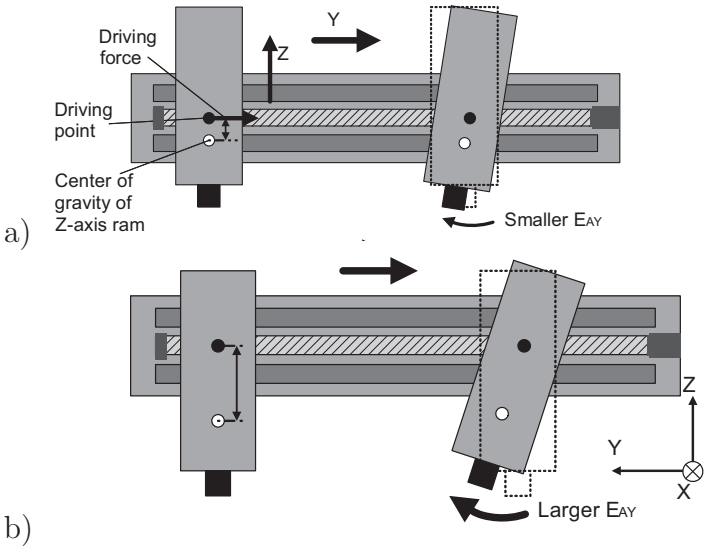


Figure 4: Possible influence of Z-position on the pitch error motion of Y-axis, $E_{AY}(y)$.

Such an influence cannot be described in the conventional model (1). For the machine configuration shown in Fig. 2, where the Z-axis is mounted on the Y-axis, possible axis cross-talks are as follows:

1) As illustrated in Fig. 4, the Z-axis position changes the position of the center of gravity of the Z-axis ram with respect to the Y-axis driving point. The pitch error motion of Y-axis, $E_{AY}(y)$, can be influenced by the friction on the two Y-axis guideways, and thus the Z-position may influence it. 2) As illustrated in Fig. 5, the Z-axis position may also change the roll error motion of Y-axis, $E_{BY}(y)$. The Y-axis roll error motion can be caused by the rotation of the Y-axis ball screw with the elastic deformation of guide way, and thus its deformation may be dependent to the distance from the ball screw centerline to the center of gravity of Z-axis ram.

*2.3. Direction- and velocity-dependent error motions*

The term "backlash" typically represents the direction-dependent difference in the linear positioning error motion. Particularly on large-sized machines, where the friction on a guideway or a ball screw can have significant

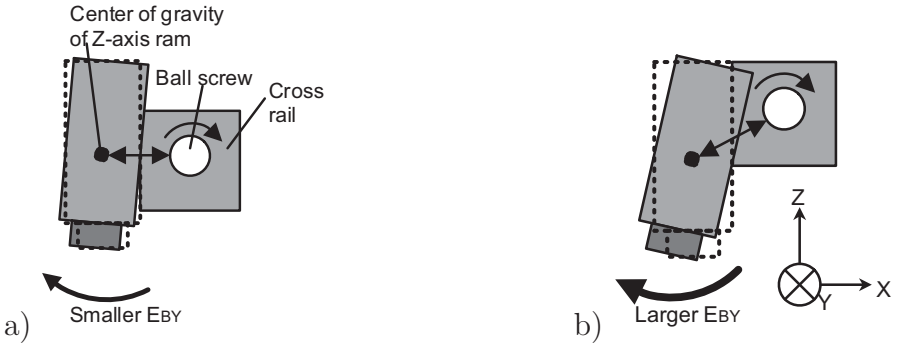


Figure 5: Possible influence of Z-position on the roll error motion of Y-axis, $E_{BY}(y)$.

influence on error motions, all the six error motions of a linear axis may be dependent on the direction of the motion. As an example, Fig. 6 shows possible influence of the Y-axis feed direction on the pitch error motion of Y-axis, $E_{AY}(y)$.

Furthermore, error motions may significantly vary with the feed speed. For example, when the Y-axis pitch error motion, $E_{AY}(y)$, is affected by the guideway friction, it likely depends on the feed speed.

### *2.4. Extended kinematic model*

The influence discussed in Section 2.2 can be included in the kinematic model in Eq. (1) by simply defining the error motions, $E_{AY}(y)$ and $E_{BY}(y)$, dependent not only the command Y-position, $y$, but also the command Z-position, $z$, i.e. $E_{AY}(y, z)$ and $E_{BY}(y, z)$. Similarly, the influence discussed in Section 2.3 can be modelled by defining $E_{AY}(y)$ dependent also on the direction of $y$, $\mathrm{sgn}(\dot{y})$, where $\mathrm{sgn}(\dot{y}) \equiv +1$ when $\dot{y} > 0$ and $-1$ when $\dot{y} \leq 0$.

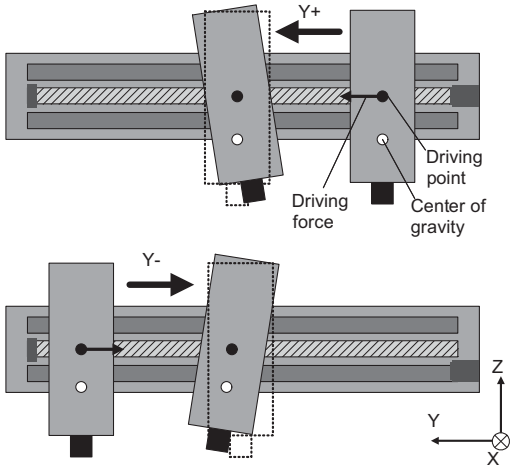


Figure 6: Possible influence of the Y-axis feed direction on the pitch error motion of Y-axis, $E_{AY}(y)E_{AY}(y)$.

The extended kinematic model can be written by:

$$\begin{aligned}
e_x(x,y,z) &= E_{XX}(x,\mathrm{sgn}(\dot{x}),\dot{x}) + E_{XY}(y,z,\mathrm{sgn}(\dot{y}),\dot{y}) + E_{XZ}(z,\mathrm{sgn}(\dot{z}),\dot{z}) \\
&\quad - \left(E_{CX}(x,\mathrm{sgn}(\dot{x}),\dot{x}) + E_{C(0X)Y}\right) y \\
&\quad - \left(E_{BX}(x,\mathrm{sgn}(\dot{x}),\dot{x}) + E_{BY}(y,z,\mathrm{sgn}(\dot{y}),\dot{y}) + E_{B(0X)Z}\right) z \\
e_y(x,y,z) &= E_{YX}(x,\mathrm{sgn}(\dot{x}),\dot{x}) + E_{YY}(y,z,\mathrm{sgn}(\dot{y}),\dot{y}) + E_{YZ}(z,\mathrm{sgn}(\dot{z}),\dot{z}) \\
&\quad + E_{CX}(x,\mathrm{sgn}(\dot{x}),\dot{x}) \cdot x \\
&\quad - \left(E_{AX}(x,\mathrm{sgn}(\dot{x}),\dot{x}) + E_{AY}(y,z,\mathrm{sgn}(\dot{y}),\dot{y}) + E_{A(0Y)Z}\right) z \\
e_z(x,y,z) &= E_{ZX}(x,\mathrm{sgn}(\dot{x}),\dot{x}) + E_{ZY}(y,z,\mathrm{sgn}(\dot{y}),\dot{z}) + E_{ZZ}(z,\mathrm{sgn}(\dot{z}),\dot{z}) \\
&\quad - E_{BX}(x,\mathrm{sgn}(\dot{x}),\dot{x}) \cdot x + E_{AX}(x,\mathrm{sgn}(\dot{x}),\dot{x}) \cdot y \qquad (2)
\end{aligned}$$

## 3. Proposed test procedure

A 2D digital scale (the term in [3]), or a cross grid encoder [12], continuously measures the 2D coordinate position of a 2D scale detector, attached to a machine spindle, relative to a reference 2D scale (grid scale) fixed on a machine table (see Fig. 7). The proposed test procedure is as follows:

(1) On the YZ plane: the reference grid plate is fixed approximately on the YZ plane in the position, Setup YZ-1, in Fig. 7 a-1). The dimensions in Fig. 7 a-1) to c-1) show the experimental setup in Section 5 and are examples only. Fig. 7 a-2) shows actual test setup in the experiment.
Then, 2D contour error for the paths shown in Fig. 8 are measured, a) square path, b) straight paths, and 3) L-shaped paths. The paths a) and b) should be measured bi-directionally. The paths b) should be measured under different feed speeds. The travel, $a$ in Fig. 8, should be chosen as large as possible within the 2D digital scale's measuring range. In the experiment, $a$ = 160 mm. This is repeated at Setups YZ-1 and YZ-2 in Fig. 7 a-1).
(2) On the XY plane: the reference grid plate is fixed at Setups XY-1 and XY-2 in Fig. 7 b-1), and the same paths are measured on the XY plane.
(3) On the XZ plane: the reference grid plate is fixed at Setups XZ-1 to XZ-4 in Fig. 7 c-1), and the same paths are measured on the XZ plane.

## 4. Assessment of error motions

### *4.1. Quasi-static position-dependent error motions: Error motions contained in conventional rigid-body kinematic model*

At each setup, *local* error motions of each linear axis involved, i.e. linear positioning, straightness and angular error motions of two linear axes, can be assessed within the measuring range, i.e. for the travel, $a$ in Fig. 8. This assessment can be done according to ISO 230-1 [3]. This is usually not very informative, since the measuring range of a 2D digital scale is often much smaller than the machine tool's linear axis strokes.

This paper's first contribution is on the assessment of angular error motions by comparing multiple trajectories measured at different positions. As an example, Fig. 9 illustrates the influence of Y-axis roll error motion, $E_{BY}(y)$, on the squareness error of Z- to X-axis, $E_{B(0X)Z}$, at different Y positions. When $E_{B(0X)Z}$, measured at Setups XZ-1 and XZ-2 in Fig. 7 c-1),

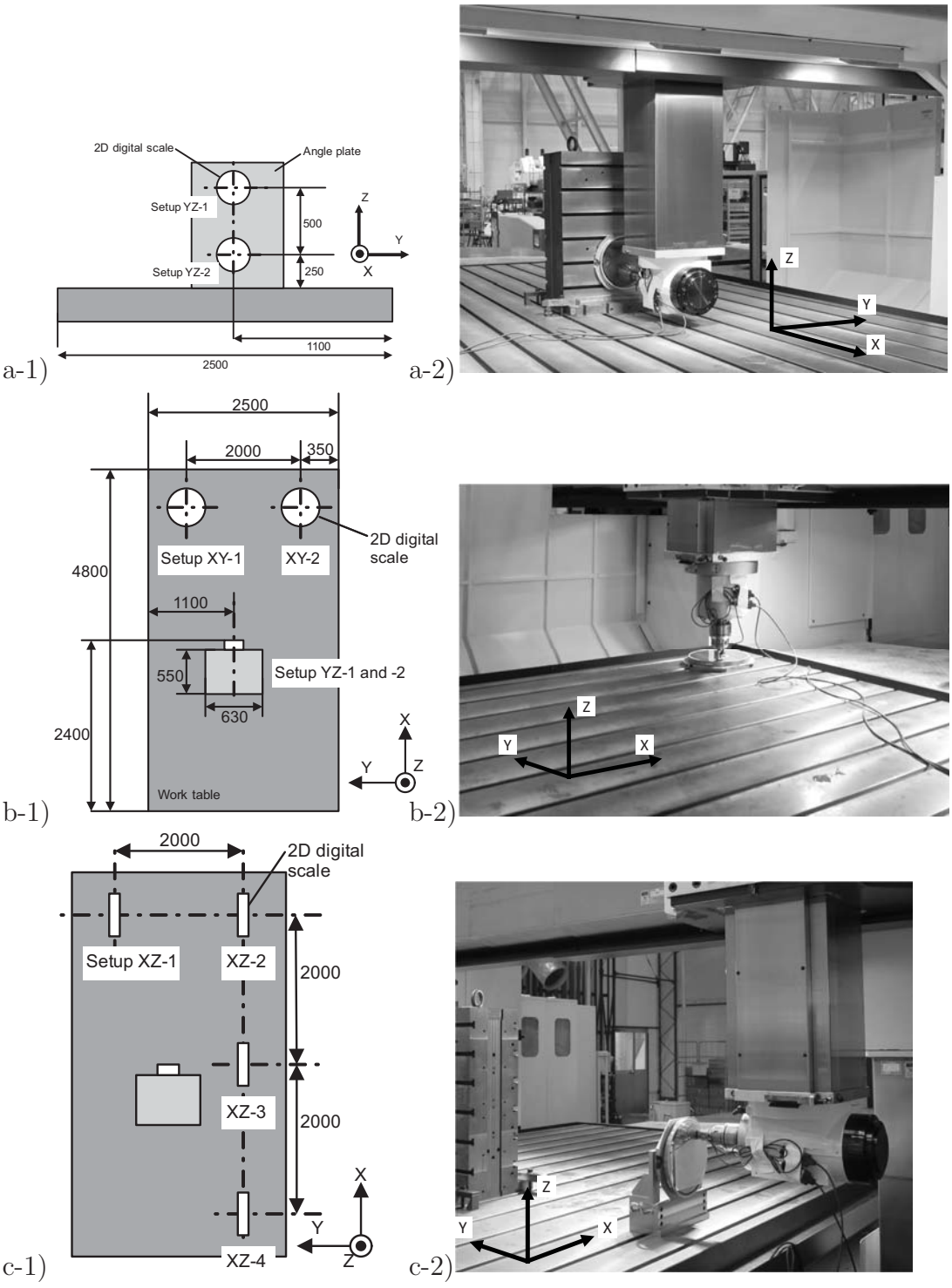




Figure 7: 2D digital scale setups in the proposed test procedure. a-1) Setups YZ-1 and YZ-2 for the YZ plane. a-2) Actual test setup (Setup YZ-2). b-1) Setups XY-1 and XY-2 for the XY plane. b-2) Actual test setup (Setup XY-1). c-1) Setups XZ-1 to XZ-4 for the XZ plane. c-2) Actual test setup (Setup XZ-3).

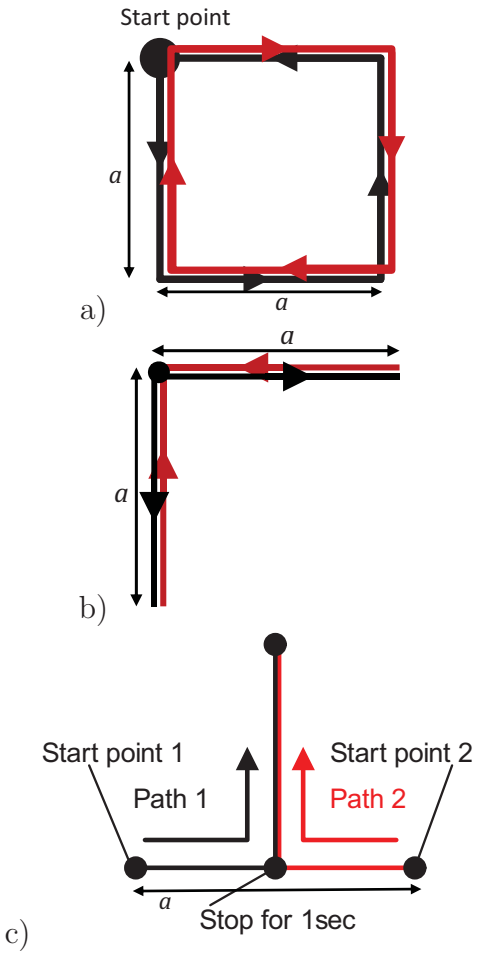


Figure 8: Test paths. a) Square path (bidirectional), b) straight paths (bidirectional), and c) L-shaped paths. b) should be repeated with different feed speeds.

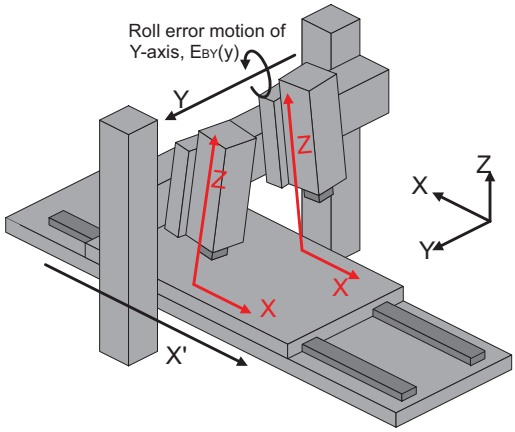


Figure 9: Influence of Y-axis roll error motion, $E_{BY}(y)$, on the squareness error of Z- to X-axis at different Y positions.

Table 1: Assessment of angular error motions by comparing multiple tests. †: possible to assess, but not included in the proposed tests.

| Error motions | Assessment |
|---|---|
| Pitch of X-axis, $E_{BX}(x)$ | Comparison of Setups XZ-2, -3 and -4 |
| Yaw of X-axis, $E_{CX}(x)$ | (Comparison of measurements on XY plane at different X positions)† |
| Roll of Y-axis, $E_{BY}(y)$ | Comparison of Setups XZ-1 and -2 |

are denoted by $E_{B(0X)Z}(y_1)$ and $E_{B(0X)Z}(y_2)$, then the change in the Y-axis roll error motion is given by

$$E_{BY}(y_1) - E_{BY}(y_2) = E_{B(0X)Z}(y_1) - E_{B(0X)Z}(y_2) \tag{3}$$

The distance between the two setups, $y_2 - y_1$, can be much larger that a 2D digital scale's measuring range (2,000 mm in the experiment).

The kinematic model (1) contains five angular error motions. Table 1 summarizes the assessment of three angular errors by comparing the squareness error measured at multiple positions.

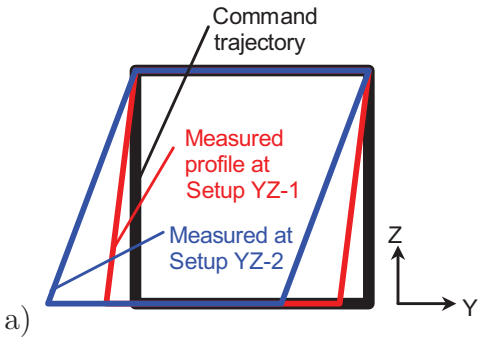


Figure 10: An illustrative example of the influence of the pitch error motion of Y-axis, $E_{AY}(y, z)$, changed with the Z position, on contour error profiles on the YZ plane at Setups YZ-1 and YZ-1 (at different Z positions).

### *4.2. Quasi-static cross-talk between axes*

Possible influence of Z-axis position on the pitch error motion of Y-axis, $E_{AY}(y, z)$, illustrated in Fig. 4, changes contour error profiles measured at Setups YZ-1 and YZ-2 (YZ plane tests at different Z positions) as illustrated in Fig. 10. Therefore, where the Y-Z squareness errors at Setups YZ-1 and YZ-2 are denoted by $E_{A(0Y)Z}(z_1)$ and $E_{A(0Y)Z}(z_2)$, then the difference in the Y-axis pitch error motion at different Z positions can be assessed by

$$E_{AY}(y, z_1) - E_{AY}(y, z_2) = E_{A(0Y)Z}(z_1) - E_{A(0Y)Z}(z_2) \tag{4}$$

This paper's second contribution is on this measurement and assessment procedures.

**Remark:** An alternative way to observe this influence is to directly measure the Y-axis pitch error motion, $E_{AY}(y, z)$, at different Z positions, $z_1$ and $z_2$. The proposed test procedure enables a user to assess all the error motions by using a 2D digital scale only. But other measuring instruments can be applied.

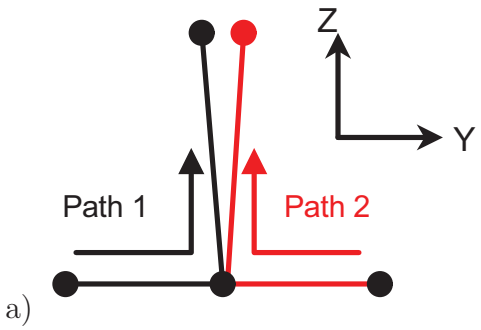


Figure 11: An illustrative example of the influence of the pitch error motion of Y-axis, $E_{AY}(y, \mathrm{sgn}(\dot{y}))$, changed with the Y-axis feed direction, on contour error profiles for the L-shaped paths on the YZ plane.

### *4.3. Direction- and velocity-dependent error motions*

By measuring straight paths path in Fig. 8 b), direction-dependent linear positioning and straightness error motions of each linear axis can be assessed within the measuring range. This is contained in standardized accuracy tests in ISO 230-1 [3].

This paper's third contribution is on the assessment of direction-dependent angular error motions by measuring the L-shaped paths in Fig. 8 c). When the Y-axis pitch error motion, $E_{AY}(y, \mathrm{sgn}(\dot{y}))$, is changed by the Y-axis feed direction, it changes the direction of Z-axis moved after the Y-axis, as illustrated in Fig. 6. This results in the difference in the contour error as illustrated in Fig. 11. When the Y-Z squareness errors for the left and right L-shaped paths are denoted by $E_{A(0Y)Z}(\mathrm{left})$ and $E_{A(0Y)Z}(\mathrm{right})$, then the change in the Y-axis pitch error motion by the Y-axis feed direction is calculated by:

$$E_{AY}(y, +1) - E_{AY}(y, -1) = E_{A(0Y)Z}(\mathrm{right}) - E_{A(0Y)Z}(\mathrm{left}) \tag{5}$$

Table 2: Major specifications of the machine tool.

| | |
|---|---|
| Travel | X:5,000 mm, Y:3,700 mm<br>Z: 800 mm, W:1,300 mm |
| Drive | Servo motor and<br>ball screw (all axes) |
| Guideway | X, Y: Roller/slide guideway<br>Z: Slide guideway |
| Positioning<br>resolution | 0.1 $\mu$m<br>(all axes) |

Table 3: Major specifications of the 2D digital scale (KGM282 by Heidenhain) [22].

| | |
|---|---|
| Measuring standard | Two-coordinate TITANID<br>phase grating |
| Measuring range | $\phi$230 mm |
| Accuracy grade | $\pm 1\mu$m |
| Signal period | 4 $\mu$m in two directions |

## 5. Case study

### *5.1. Experimental setup*

A commercial machining center of the configuration shown in Fig. 2 was tested. Table 2 shows its major specifications. A 2D digital scale, KGM282 by Heidenhain, was used. Its specifications are shown in Table 3. See Fig. 7 for the test setups.

### *5.2. Quasi-static position-dependent error motions*

First, a single test is analyzed as discussed in Section 4.1. As an example, Fig. 12 shows the contouring error profile on the XZ plane measured at Setup XZ-1 in Fig. 7 c-1). In all the contour error plots in this paper, an error from the command trajectory to the measured trajectory is magnified 10,000 times, i.e. 50 mm in the plot corresponds to an error of 5 $\mu$m (see

"Error scale"). The arrows shows the feed direction.
**Note:** An error is magnified in the direction normal to the command trajectory. In Fig. 12, the measured trajectory seems disconnected at the corners. This is because the error is magnified in a different direction at each edge. The actual trajectory is continuous.

Table 4 shows a test report for the measured trajectory in Fig. 12, summarizing error motions of X- and Z-axes observed from it. As was discussed in Section 4.1, this only shows *local* error motion within the measuring range, $a = 160$ mm. Analogous test reports can be made for the YZ plane (e.g. Setup YZ-1) and the XY plane (e.g. Setup XY-1).

Then, linear axis angular error motions are assessed by comparing multiple tests. Figure 13 compares the measured profiles in Setups XZ-1 and XZ-2. As depicted in Fig. 9, the Y-axis roll error motion, $E_{BY}(y)$, can be assessed by the difference in the Z-X squareness error at two Y positions. Table 5 shows its test report.

Analogously, the pitch error motion of X-axis, $E_{BX}(x)$, can be assessed by comparing measured profiles at Setups XZ-2, -3 and -4. Its report is omitted here.

### *5.3. Quasi-static cross-talk between axes*

Figure 14 compares contouring error profiles measured at Setup YZ-1 and YZ-2 (YZ plane tests at different Z positions). It shows that the Y-Z squareness error is different at different Z positions. As illustrated in Fig. 10, this can be caused by the influence of Z-axis position on the pitch error motion of Y-axis, $E_{AY}(y, z)$ (see Fig. 4). Table 6 shows its test report.

### *5.4. Direction- and velocity-dependent error motions*

By bidirectional measurement for the straight path (Fig. 8 b), the direction-dependent error motions can be assessed. As an example, Fig. 15 shows contouring error profiles on the XZ plane for the bidirectional straight path to the Z-direction, measured at Setup XZ-3. It shows that the Z-axis straightness error motion, $E_{XZ}(z, \mathrm{sgn}(\dot{z}))$, significantly differs in positive and negative

feed directions, which is probably attributable to the direction-dependent angular error motion of Z-axis, $E_{AZ}(z, \dot{z})$. Table 7 shows its test report.

Analogous test reports can be made for X-axis (in Y at Setup XY-1, in Z at Setup XZ-3), Y-axis (in X at Setup XY-1, in Z at Setup YZ-2), and Z-axis (in X at Setup XZ-3, in Y at Setup YZ-2) but omitted here. Such assessment is included in standard accuracy tests in ISO 230-1 [3].

A new contribution of this paper is on the assessment of direction-dependent angular error motions. Figure 16 shows contouring error profiles for the L-shaped path (Fig. 8 c) on the XY plane (at Setup XY-2). Only contour error profiles for the vertical path are shown, with horizontal profiles aligned to the X-direction. A slight difference in their orientations can be observed, which shows the difference in the yaw error motion of X-axis for different directions, $E_{CX}(x, +1) - E_{CX}(x, -1)$. Table 8 shows its test report.

Analogous test reports can be made for X-axis (pitch, $E_{BX}(x, \mathrm{sgn}(\dot{x}))$, at Setup XY-3) and Y-axis (pitch, $E_{AY}(y, \mathrm{sgn}(\dot{y}))$, at Setup YZ-2).

Velocity-dependent error motions can be assessed by performing the tests under different feed speeds. As an example, Fig. 17 shows contouring error profiles for the square path on the YZ plane (at Setup YZ-2) under the feed speeds 500 and 10,000 mm/min. Under the higher feed speed, the TCP was elevated to +Z direction by about 4 $\mu$m at maximum, as the Y-axis moves. This is probably attributable to the lubrication on the slide guideway of Y-axis. Table 9 shows its test report.

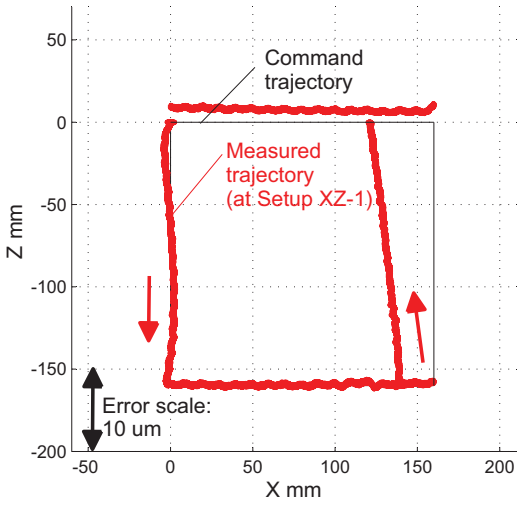


Figure 12: Contouring error profile on the XZ plane measured at Setup XZ-1. The error from the command trajectory to the measured trajectory is magnified 10,000 times (see "Error scale"). The arrows shows the feed direction.

Table 4: Test report: a single test at Setup XZ-1 (measured profile: Fig. 12).

| Error motion | Measured range (mm) | Value |
|---|---|---|
| Squareness error of Z to X, $E_{B(0X)Z}$ | at $(x, z)$=(-362, 593) | -7.5 $\mu$m/m |
| Linear positioning deviation of X, $E_{XX}(x)$ | $x = -362$ to -202 | -7.3 $\mu$m |
| Linear positioning deviation of Z, $E_{ZZ}(z)$ | $z = 433$ to 593 | 0.4 $\mu$m |
| Straightness error of X, $E_{ZX}(x)$ | $x = -362$ to -202 | 1.3 $\mu$m |
| Straightness error of Z, $E_{XZ}(z)$ | $z = 433$ to 593 | 1.9 $\mu$m |
| Pitch error motion of X, $E_{BX}(x)$ | $x = -362$ to -202 | -18.6 $\mu$m/m |

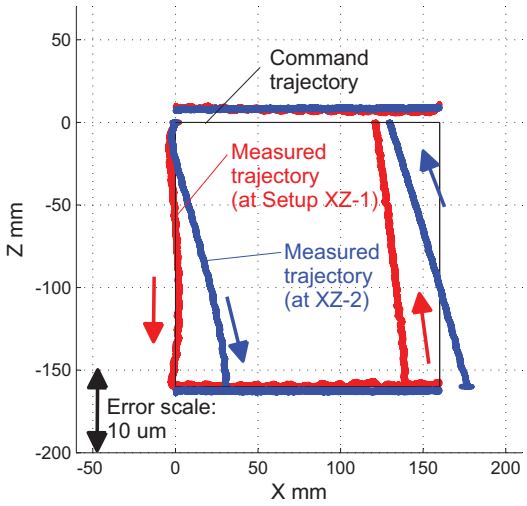


Figure 13: Comparison of contouring error profiles on the XZ plane measured at Setups XZ-1 and XZ-2 (XZ plane tests at different Y positions).

Table 5: Test report: comparison of Setups XZ-1 and XZ-2 (measured profiles: Fig. 13).

| Error motion | Measured range (mm) | Value |
|---|---|---|
| Roll error motion of Y-axis, $E_{BY}(y)$ | $y = -200$ and 1977 | 6.8 $\mu$m/160mm |

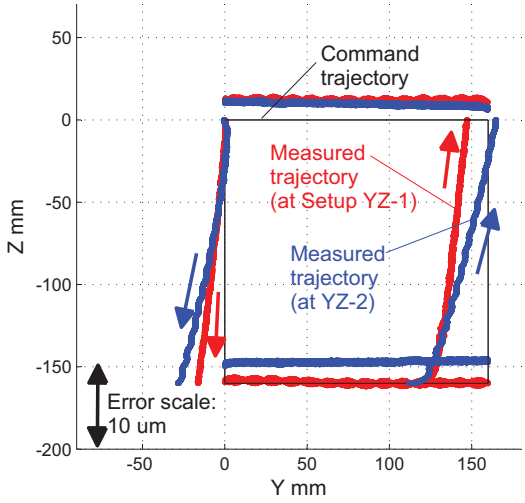


Figure 14: Contouring error profiles measured at Setup YZ-1 and YZ-2 (YZ plane tests at different Z positions).

Table 6: Test report: comparison of Setups YZ-1 and YZ-2 (measured profiles: Fig. 14).

| Error motion | Measured range (mm) | Value |
|---|---|---|
| Influence of Z-position on the pitch of Y-axis, $E_{AY}(y, z)$ | $z = -602$ and -258 | -1.9 $\mu$m/160mm |

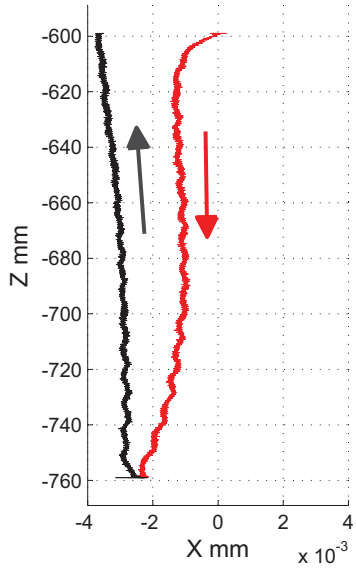


Figure 15: Contouring error profiles on the XZ plane for the bidirectional straight path to the Z-direction, measured at Setup XZ-3.

Table 7: Test report: bidirectional straight path in the Z-direction at Setup XZ-3 (measured profile: Fig. 15).

| Error motion | Measured range (mm) | Value |
|---|---|---|
| Straightness error motion of Z in X, $E_{XZ}(z, \mathrm{sgn}(\dot{z}) = +1)$ | $z = -759$ to -599 | -3.8 $\mu$m |
| Straightness error motion of Z in X, $E_{XZ}(z, \mathrm{sgn}(\dot{z}) = -1)$ | $z = -759$ to -599 | -2.4 $\mu$m |

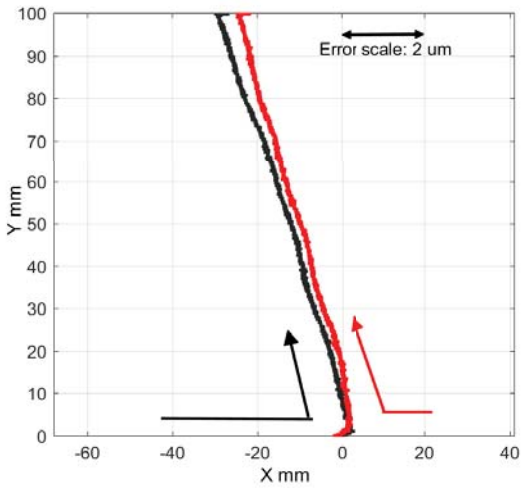


Figure 16: Contouring error profiles for the L-shaped path (Fig. 8 c) on the XY plane (at Setup XY-2). Only contour error profiles for the vertical path are shown, with horizontal profiles aligned to the X-direction.

Table 8: Test report: L-shaped paths on the XY-plane at Setup XY-2 (measured profile: Fig. 16).

| Error motion | Measured position (mm) | Value |
|---|---|---|
| Difference in yaw error motion of X for different directions, $E_{CX}(x,+1) - E_{CX}(x,-1)$ | x=281 | 0.5 $\mu$m/100mm |

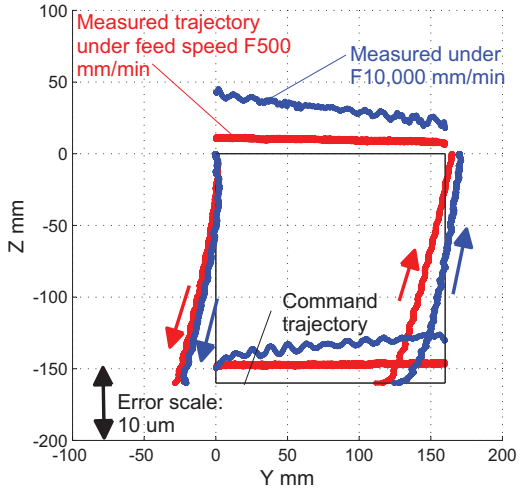


Figure 17: Contouring error profiles for the square path on the YZ plane (at Setup YZ-2) under the feed speeds 500 and 10,000 mm/min.

Table 9: Test report: Comparison of the square paths on the YZ plane at Setup YZ-2 under feed speeds 500 and 10,000 mm/min (measured profile: Fig. 17).

| Error motion | Measured range (mm) | Value |
|---|---|---|
| Feed speed's influence on linear positioning error of Y, $E_{YY}(y, \dot{y} = 10000) - E_{YY}(y, \dot{y} = 500)$ | $y = 1335$ to 1495 | 1.2 $\mu$m |
| Feed speed's influence on linear positioning error of Z, $E_{ZZ}(z, \dot{z} = 10000) - E_{ZZ}(z, \dot{z} = 500)$ | $z = -782$ to -602 | -0.3 $\mu$m |
| Feed speed's influence on straightness error of Y, $E_{ZY}(y, \dot{y} = 10000) - E_{ZY}(y, \dot{y} = 500)$ | $y = 1335$ to 1495 | 6.9 $\mu$m |
| Feed speed's influence on straightness error of Z, $E_{YZ}(z, \dot{z} = 10000) - E_{YZ}(z, \dot{z} = 500)$ | $z = -782$ to -602 | 1.2 $\mu$m |
| Feed speed's influence on pitch error motion of Z, $E_{AY}(y, \dot{y} = 10000) - E_{AY}(y, \dot{y} = 500)$ | $y = 1335$ to 1495 | 1.5 $\mu$m/m |

## 6. Conclusion

The conventional kinematic model of a machine tool, widely used in numerical volumetric error compensation, assumes rigid-body motion and includes only (1) quasi-static error motions depending only on the axis linear position. In addition to (1), this paper presented a scheme to assess (2) quasi-static cross-talk between axes and (3) direction- and velocity-dependent error motions. ISO 230-1 [3] described standardized test procedures to assess all the error motions of linear axes, but error motions (2) cannot be assessed. This paper employs a 2D digital scale to measure contouring error profiles. This paper proposes the tests performed at multiple locations over the entire workspace.

Major novel contributions of this paper can be summarized as follows: a) the assessment of position-dependent quasi-static angular error motions by comparing contour error profiles measured at discrete positions (see Section 4.1; see Fig. 13 and Table 5 for experimental demonstration). b) The assessment of quasi-static cross-talks between axes by comparing contour error profiles measured at discrete positions (see Section 4.2; see Fig. 14 and Table 6 for experimental demonstration). c) The assessment of direction-dependent angular error motions by measuring the L-shaped paths from both directions (see Section 4.3; see Figure 16 and Table 8 for experimental demonstration). The present experimental case study showed such influences can have a significant influence on the TCP trajectory.

As a final remark, the proposed schemes a) and b) compare the two tests measured at discrete positions. These schemes can, therefore, assess the error motions only at these discrete positions. The proposed tests can be applied as accuracy inspection by machine tool builders to "roughly" assess the machine's volumetric accuracy by using a 2D digital scale only. For numerical compensation of volumetric errors, error motions should be measured over the entire stroke of each axis. The present tests are generally not for the compensation.

**Acknowledgement**

This work was in part supported by NSK Foundation for the Advancement of Mechatronics in 2016. Heidenhain supported this study by providing a 2D digital scale, KGM282. The authors acknowledge their support.

**References**

[1] Longstaff AP, Fletcher S, Myers A. Volumetric error compensation through a Siemens controller, Laser Metrology and Machine Performance VII 2005: 422-431.

[2] Yamada Y. Compensation technology for volumetric error in Machine Tool, Proc. of the 15th International Machine Tool Engineers' Conference 2012.

[3] ISO 230-1:2012, Test code for machine tools – Part 1: Geometric accuracy of machines operating under no-load or quasi-static conditions.

[4] ISO/TR 16907:2015, Numerical compensation of geometric errors of machine tools.

[5] Reshetov DN, Portman VT. Accuracy of Machine Tools, ASME Press, 1988.

[6] Creamer J, Sammons PM, Bristow DA, Landers RG, Freeman PL, Easley SJ. Table-Based Volumetric Error Compensation of Large Five-Axis Machine Tools, Journal of Manufacturing Science and Engineering, 2016: 139(2): 021011/11.

[7] Li Z, Feng W, Yang J, Huang Y. An investigation on modeling and compensation of synthetic geometric errors on large machine tools based on moving least squares method, Proc. of the Institution of Mechanical Engineers, Part B: Journal of Engineering Manufacture, 2016: 232(3): 412-427.

[8] Li J, Mei B, Shuai C, Liu X, Liu D. A volumetric positioning error compensation method for five-axis machine tools, International Journal of Advanced Manufacturing Technology, 2019: 103(9-12): 3979-3989.

[9] Abbaszaheh-Mir Y, Mayer JRR, Clotier G, Fortin C. Theory and simulation for the identification of the link geometric errors for a five-axis machine tool using a telescoping magnetic ball-bar, International Journal of Production Research, 2002; 40(18): 4781–4797.

[10] Schwenke H, Franke M, Hannaford J, Kunzmann H. Error mapping of CMMs and machine tools by a single tracking interferometer, CIRP Annals – Manufacturing Technology, 2005: 54(1): 475-478.

[11] Mayer JRR. Five-axis machine tool calibration by probing a scale enriched reconfigurable uncalibrated master balls artefact, CIRP Annals – Manufacturing Technology, 2012: 61(1): 515-518.

[12] Du Z, Zhang S, Hong M. Development of a multi-step measuring method for motion accuracy of NC machine tools based on cross grid encoder, International Journal of Machine Tools and Manufacture, 2010: 50(3):270-280

[13] Ibaraki S, Tsujimoto S, Nagai Y, Sakai Y, Morimoto S, Miyazaki Y, A pyramid-shaped machining test to identify rotary axis error motions on five-axis machine tools: Software development and a case study, International Journal of Advanced Manufacturing Technology, 2018: 94(1): 227-237.

[14] Schwenke H, Knapp W, Haitjema H, Weckenmann A, Schmitt R, Delbressine F (2008) Geometric Error Measurement and Compensation of Machines – An Update. CIRP Annals – Manufacturing Technology 2008; 57(2):560-575.

[15] Ibaraki S, Knapp W, Indirect Measurement of Volumetric Accuracy for

Three-axis and Five-axis Machine Tools: A Review, International Journal of Automation Technology 2012; 6 (2):110-124.

[16] Uriarte L, Zatarain M, Axinte D, Yagüe-Fabra J, Ihlenfeldt S. Eguia J, Olarra A. Machine tools for large parts, CIRP Annals–Manufacturing Technology, 2013: 62(2): 731-750.

[17] Bringmann B, Maglie P. A method for Direct Evaluation of the Dynamic 3D Path Accuracy of NC Machine Tools, CIRP Annals - Manufacturing Technology, 2009: 58(1): 343-346.

[18] Kono D, Lorenzer T, Weikert S, Wegener L. Evaluation of Modelling Approaches for Machine Tool Design, Precision Engineering, 2010: 34: 399-407.

[19] ISO 10791-1:2015, Test conditions for machining centres – Part 1: Geometric tests for machines with horizontal spindle (horizontal Z-axis)

[20] Knapp W, Weikert S. Testing the contouring performance in 6 degrees of freedom, Annals of the CIRP, 1999: 48(1): 433-436.

[21] Boye T, Günther G, Fritz M. Increasing 5-axis accuracy by using a cross grid encoder for volumetric compensation, Laser Metrology and Machine Performance XI, 2015: 61-70.

[22] Encoders for Machine Tool Inspection and Acceptance Testing, Heidenhain catalog, 09/2017.